Association Aéronautique et Astronautique de France

57th 3AF International Conference on Applied Aerodynamics
29 – 31 March 2023, Bordeaux - France

AERO2023-34

DYNAMIC GUST LOAD ALLEVIATION STUDY WITH SURROGATE MODELS FOR TRANSONIC CRUISE CONDITION

Kuharaaj Govindan [(1)]

[(1)]*Research Engineer, Department of Transport Aircraft, Institute of Aerodynamics and Flow Technology, German Aerospace Center (DLR), Braunschweig, D-38108, Germany, Email: kuharaaj.govindan@dlr.de*

ABSTRACT

This study aims to predict dynamic responses of trailing-edge and droop-nose devices in 2D for a transonic cruise condition using surrogate models. The prepared surrogates, also known as reduced order models, were prepared using the Linear Frequency Domain solver, and are proven to provide quick results for a wide range of flight conditions while being computationally efficient. Three reduced order models were prepared, one for predicting gust load responses for given gust cases, a second purely to predict trailing-edge deflection dynamics responses, and a third to prognose droop-nose device deflection dynamic response. Each surrogate was modelled with 100 dynamic response results based on their respective parameter combinations, prepared as a Halton Sequence of points. The prepared surrogates were evaluated for quality of interpolation via the Leave-One-Out Test, and applied for prognosing three flight cases. The superposition principle was applied to combine the dynamic responses from each surrogate to evaluate the load mitigation capability of the trailing-edge and droop nose devices for the studied flight cases. The surrogate predictions were accurate within -2 orders of magnitude relative to conventional unsteady flow simulations and the results of this gust load alleviation study with the reduced order models are comparable to other studies. This study proves the applicability of surrogate models prepared with the Linear Frequency Domain method, as a knowledge-based engineering approach, to perform aerodynamic studies, relevant to conceptual research as well as industrial needs.

1. NOMENCLATURE

AoA	:	Angle of attack
c_l	:	Section lift coefficient
c_d	:	Section drag coefficient
c_m	:	Section moment coefficient
DND	:	Droop-nose device
f	:	Frequency
im	:	Imaginary part of complex number
k	:	Reduced frequency
l_{ref}	:	Reference length
Ma	:	Mach number
n	:	Harmonic / Mode
$\boldsymbol{R}$	:	Residuals
Re	:	Reynolds number
re	:	Real part of complex number
TED	:	Trailing-edge device
t	:	Time
$\boldsymbol{u}$	:	State vectors
v_∞	:	Free stream velocity
$\boldsymbol{x}$	:	Grid coordinates
δ	:	Control surface deflection angle
ρ	:	Density
φ	:	Phase shift
ω	:	Angular velocity
ω_b	:	Base angular velocity

2. INTRODUCTION

Gust encounters during flight influence the aerodynamics, flight mechanics and aeroelastics of the aircraft, affecting the structure as well [12]. As of such, aircrafts must always be designed, with gust load conditions in mind.

Considering also the ever-increasing need to reduce fuel consumption, more efficient wings become an interesting prospect. Higher aspect-ratio wings promote less drag [8][5], however, longer wings also

mean larger wing bending moments at the root, necessitating structural reinforcements, which, naturally add weight, and require more energy, ergo, fuel, to fly. To circumvent this problem, correct spanwise load distribution, and in fact, load distribution control is crucial, as detailed by Xu [13]. Maintaining a structural load equal to non-accelerated (1g) flight ensures structural weight increase remain minimal. Considering different load cases during flight, especially gusts, active load alleviation technology, besides passive ones, become relevant. The former, is the main topic of study here.

Effort have been made in line with this goal with promising results. Hübner and Reimers simulated a generic aircraft counteracting gust loads with ailerons using unsteady Reynolds-averaged Navier-Stokes (URANS) techniques [7], achieving ~20% load alleviation with the said device. Ullah et.al. [10] conducted steady and unsteady RANS studies for the full span of a wing to investigate flap and droop-nose device gust load mitigation capabilities. Their study showed that a trailing-edge device application in gust load alleviation (GLA) required the use of a droop-nose device so as to not amplify wings torsional loads during gusts. They concluded that up to 58% of GLA was possible via a steady and dynamic combination of flap and droop-nose device deflections during transonic cruise flight. These results prove valuable; however, the use of standard URANS techniques is computationally tedious and thereby the number of possible scenarios for investigation become limited. This discourages the sole use of the URANS method for predictive studies to determine ideal device deflections for gust load alleviation.

This work seeks to implement the use of surrogate modelling to predict the control surface deflections necessary for optimal GLA. The model's database is to comprise of high-fidelity solutions in the frequency domain, prepared with a linear frequency domain (LFD) solver. If applicable, computational efficiency for the said purpose of GLA studies can be vastly enhanced [4] along with the number of investigation possibilities and variations in GLA. This work considers two high-lift-devices in 2D: a trailing-edge device and a droop-nose device; the trailing-edge device, such as an aileron, simple flap or a flap-tab functions to counteract any lift increment due to gust, while the droop-nose could be deployed to alleviate changes in pitching moment due to trailing edge deflections. Surrogate models were used to predict these dynamic loads resulting from gusts, as well as the required device's deflection profiles. The surrogates, also called reduced order models, or ROMs for short, were designed for the cruise condition with the following dimensions: Mach number, Ma, Flight Level, FL, angle of attack, AoA, and the mean angle of device deflection. In total, 3 surrogates were prepared: one prognosed the dynamic gust loads for a clean configuration; the second, the required trailing-edge device deflection profile to counter the loading influence of gusts; while a third, predicted the droop-nose deflection profile and its contribution to the changes in wing-section pitching moments. The gust load alleviation prognoses were conducted step-by-step through the sequence of ROMs listed above; all three ROMs thereby acted together as a coupled system, in order to evaluate the load mitigation of any given flight case.

3. METHODOLOGY

3.1. The RANS-LFD Method

The RANS-LFD technique approaches the problem of computing/predicting dynamic flow field behavior via modelling the flow field as a simple harmonic oscillator. The concern of the method is thereby the modes of oscillation present in the turbulent flow field and not the actual flow physics, best described by the Navier-Stokes equations. To model the flow field purely as an oscillating harmonic system, Fourier analysis is used. The following are the standard set of procedures used to decompose the flow field system into its modes of oscillation with Fourier:

Eq. 1 describes the governing equation of an unsteady flow field in a semi-discrete form:

$$\frac{d\boldsymbol{u}}{dt} + \boldsymbol{R}(\boldsymbol{u}, \boldsymbol{x}, \dot{\boldsymbol{x}}) = 0 \qquad (1)$$

The conservation criterion of the flow field is maintained: all state-vectors, $\boldsymbol{u}$, are conserved; with the system residuals, $\boldsymbol{R}(\boldsymbol{u}, \boldsymbol{x}, \dot{\boldsymbol{x}})$, equaling in magnitude the temporal variations of $\boldsymbol{u}$.

As the system is dynamic, should the oscillations be small, the flow field can be described as small perturbations super-positioned over a mean steady state:

$$\boldsymbol{u}(t) = \bar{\boldsymbol{u}} + \tilde{\boldsymbol{u}}(t) \quad \|\tilde{\boldsymbol{u}}\| \ll \|\bar{\boldsymbol{u}}\| \qquad (2)$$

$$\boldsymbol{x}(t) = \bar{\boldsymbol{x}} + \tilde{\boldsymbol{x}}(t) \quad \|\tilde{\boldsymbol{x}}\| \ll \|\bar{\boldsymbol{x}}\| \qquad (3)$$

This decomposition leads to two things: firstly, that the flow can be solved in two parts: a mean steady state section can be computed via the standard RANS simulation method. Only the second part, the small perturbation component, needs now to be addressed. The conventional technique of solving

the problem would be via turbulence models; here, however, Fourier is utilized to decompose the perturbations into their respective modes:

$$\boldsymbol{u}(t) = \bar{\boldsymbol{u}} + \sum_n \hat{\boldsymbol{u}}_n e^{in\omega_b t} \quad (4)$$

$$\boldsymbol{x}(t) = \bar{\boldsymbol{x}} + \sum_n \hat{\boldsymbol{x}}_n e^{in\omega_b t} \quad (5)$$

Eq. 4 and 5 can be applied to Eq. 1 to produce a final model of the dynamic flow behavior, which is the response of the flow field on a specific perturbating frequency:

$$\left\{in\omega_b \boldsymbol{I} + \frac{\partial \boldsymbol{R}}{\partial \boldsymbol{u}}\right\}\hat{\boldsymbol{u}}_n = -\frac{\partial \boldsymbol{R}}{\partial \boldsymbol{x}}\hat{\boldsymbol{x}}_n - in\omega_b \frac{\partial \boldsymbol{R}}{\partial \dot{\boldsymbol{x}}}\hat{\boldsymbol{x}}_n \quad (6)$$

Eq. 6 simply states that the flow field (state vectors, $\hat{\boldsymbol{u}}_n$) responds linearly to the harmonic motion of the grid space. Depending on the modes present in the oscillating system; though these modes may be numerous, the approach is simplified by considering a system where the first harmonic alone is dominant.

Numerically, the right-hand-side (RHS) of Eq. 6 is modelled with physically feasible values to best describe the flow system under investigation: The state-vectors, $\hat{\boldsymbol{u}}_n$, are then solved in the left-hand-side (LHS) of Eq. 6 iteratively. Readers interested in a rigorous derivation of Eq. 6 are herewith directed to the works by Widhalm and Thormann [11] in the literature reference.

3.2. Surrogate Modelling with RANS-LFD

The following describes the reasoning and process of surrogate modeling with RANS-LFD:

To simplify the solving of Eq. 6, the first harmonic is taken as dominant in the flow field; this requires simulating a scenario where the assumption that the response amplitude is linear with the perturbation holds true. However, as any given component deflection is realistically composed of a multitude of harmonics, these too would need to be considered.

In order to do this, Eq. 6 is run in a series, for a range of harmonics. The compilation of these harmonics can be used as a database, to later superimpose those relevant harmonics, to describe the dynamic behavior of the flow field due to an arbitrary disturbance. Due to the linearity condition of Eq. 6, the relevant frequencies are derived directly from the component deflection itself using a Fast Fourier Transform (FFT); these, in turn, correspond linearly to the dynamic behavior of the flow field.

For a range of flight conditions, a series of such dynamic flow data for a relevant frequency range can be collected: with such a data-cloud, for any given flight condition, and decomposed frequencies of a component's deflection, the aerodynamic data can be superimposed to predict the dynamic response of the flow field. Each data-point in the mentioned data-cloud is known as a snapshot.

The range of frequencies chosen should incorporate all plausible modes for the description of any component deflection, per relevance to the aerodynamic investigation: the larger the frequency range, the more refined a prediction would be possible; however, this would also mean more computational power, time and expense!

Predictions for the surrogate model were made using the DLR SMARTy Toolbox [1].

3.3. Surrogate Model's Parameter Space

The inputs necessary for the prognosis were thereby set to Mach number, Ma, flight level, FL, angle of attack, AoA, along with the component deflection profile and gust half-wavelength, H. The range for H was taken from the certification specifications for large transport aircraft §25.341 (CS 25.341) [13]. The devices in question, the droop-nose and trailing-edge devices, were each investigated for a deflection angle range as given in Table 1. The deflection angle limitations for each device were set in order to uphold the linearity condition of Eq. 6; angles beyond this range for the transonic case investigated in this study caused flow separation and were not usable for the LFD consideration. The parameter, FL, defines the temperature, pressure and density, which together with the Mach number, defines the Reynolds number, Re. This allowed for the surrogate parameter space to be made concise while describing all variables of the aerodynamic problem under investigation; it also simplifies the work of the engineer wishing to investigate a particular aerodynamic case, for a certain FL.

Two-way data interpolation is also possible with the surrogate, whereby, for a given aerodynamic response and aerodynamic case (Ma, FL, AoA), the required component deflection can be predicted.

The parameter space investigated in this study is given in Table 1:

Table 1: Surrogate Model's Parameter Space

Ma	0,67 - 0,77
FL	300 – 400
AoA [°]	1,00 - 1,96
δ_{TED} [°]	-12,5 - +3,0
δ_{DND} [°]	-5,0 - +12,5

H [m]	10 – 107

For good interpolation of values by the ROM, the data-points of the surrogate database would need to be evenly distributed across its parameter space. 100 data points were used in this surrogate, prepared as a Halton Sequence [2][6], as it produces a reliable scatter of points in the database, for interpolation.

3.4. Method of Prognosis

The initial question of how much lift increment would be generated by a gust for a given gust case, is determined by the same RANS-LFD technique, specifically formulated for gust disturbances instead of component deflection and is built-in in the DLR TAU Code. It is applied to a clean configuration of a wing section, for a series of different gust wave-lengths. This forms the first ROM of the mentioned series for predicting the wing profile gust response.

A complication arises regarding the question of predicting both trailing-edge (TED) and droop-nose (DND) devices. For LFD computation, a simplified flow-field emphasizing a single dominant harmonic, linearly related to the oscillating device, is required. Two simultaneously oscillating devices on the profile would thereby complicate the harmonic consideration of the flow field. To circumvent this problem, a superposition principle is applied: the oscillations of each device; i.e, TED and DND, were computed separately for a range of frequencies, and compiled into two separate databases. For a given gust load consideration, the required TED deflection could thereby be prognosed, and the generated wing sectional torque due to the trailing-edge-device deflection could then be used as an input for the DND-surrogate, to predict the necessary DND-deflection.

To summarize this section, three ROMs were built for the purpose of the gust load alleviation study (GLA): 1) Gust-ROM; to predict dynamic gust responses, 2) TED-ROM; to predict the trailing-edge device deflection necessary to counter the gust induced lift response, 3) DND-ROM; to predict the required droop-nose device deflection to mitigate the torque produced by the TED deflection.

Other predictions possible with the three mentioned surrogates are as follows:

1. Profile lift increments
2. Profile moment changes
3. Profile drag variation

Finally, each ROM accommodated two complimentary databases to satisfy Eq. 6: 1) the static RANS solutions and 2) the dynamic LFD solutions. In total, 14 databases of aerodynamic information were compiled in this study.

4. MODEL

4.1. Base Configuration

The study was conducted in 2D, and based on the DLR INTELWI Configuration. The 2D-profile for the study was wing section 8; taken from the wing's midsection, outboard from the engine nacelles, with good clearance from the wing tips. This was to minimize any 3D flow effects from the wing root, engines and wing tips. The profile in question is shown in Fig. 1 (not to scale):

Figure 1 Section 8 of the DLR INTELWI Configuration

4.2. 100 Profile Configurations

The clean configuration of wing section profile was used to create the base grid. The CENTAUR Mesh Generation Software by CentaurSoft was used to generate the mesh. 73 588 cells were generated. This grid was used for the Gust-ROM simulations, shown in Fig. 2.

100 different geometric configurations were needed per the deflection angles of the TED and DNDs, as outlined in Table 1. Each configuration served as a mean deflection angle, used as a reference for studying the frequency range for the device oscillations about that angle. The modification to the base model was done via a tool, written in Python. 100 different configurations of the airfoil with TED and DND deflections were thus used for the TED-ROM and the DND-ROM respectively.

The same base grid was used for the various different configurations for each TED-ROM and DND-ROM. The derived grids with deflected control surfaces were prepared by deforming the base grid according to the modified configurations using the radial-basis-function (RBF) method, built-in in TAU.

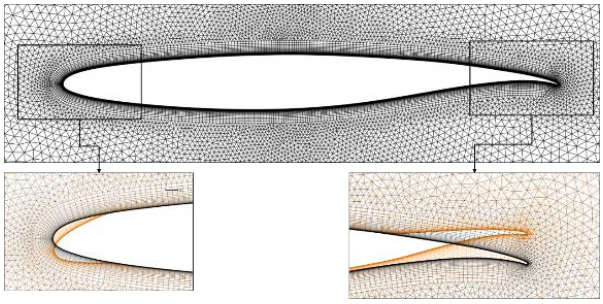

Figure 2: (Top) Base-grid for profile clean configuration of Section 8 of the INTELWI DLR

Configuration; (Bottom) Model and grid deformation for DND (bottom left) and TED (bottom right).

5. SIMULATION

5.1. RANS Solutions

To build a database of dynamic responses based on Eq. 6, the steady-mean-state solutions were prepared using the steady RANS method for each ROM. The DLR-TAU code was used for this purpose in this study, and is a Finite-Volume flow solver. The Spalart-Almaras turbulence model was the turbulence model of choice in this work, being highly applicable for a range of aerodynamic problems, and suited for this particular flow study. The simulations were each run on a single node of the DLR CARA Cluster. A residual drop up to -13 orders of magnitude provides reliable results for the LFD Method [4].

Figs. 3, 4 and 5 below shows the convergence curves of all 100 samples simulated for each ROM case, against lift coefficient normalized against cruise condition; discrepancy in the figure from an exact value of 1 is numerical:

1) Gust-ROM: 100 samples, for a target c_l for the transonic cruise condition was used, after scaling according to the wing sweep angle; the AoA for each parameter combination across the parameter space was iterated in each RANS simulation: the determined AoAs were then used to set the simulation conditions for the corresponding samples in each TED-ROM and DND-ROM computation.
2) TED-ROM: 100 samples were computed based on the 100 TED-configurations prepared as a Halton Sequence across the parameter space in Table 1.
3) DND-ROM: 100 samples were computed based on the 100 DND-configurations prepared as a Halton Sequence across the parameter space in Table 1.

All figures show a similar convergence behavior, independent of flow condition and average device deflection. For the Gust-ROM it is seen that the target lift coefficient is achieved within 6 iterations of the AoA. For any case, the convergence of -13 orders of magnitude is achieved within 4000 iterations at most.

The simulations were each run on a 64-core node of the DLR High-Performance Computing (HPC) Cluster CARA. Each RANS simulation took under 10 minutes to complete.

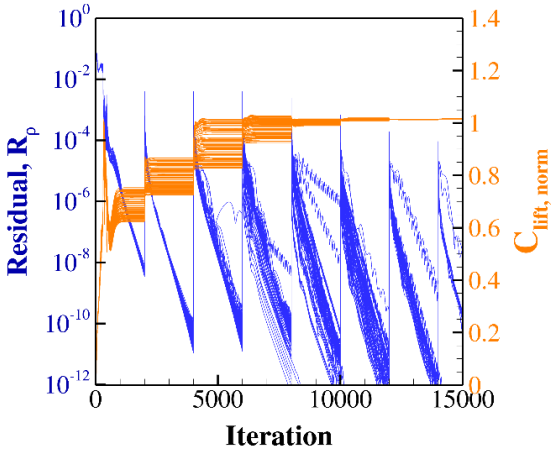

Figure 3: 100 gust-case RANS solutions; Target c_l set for cruise condition.

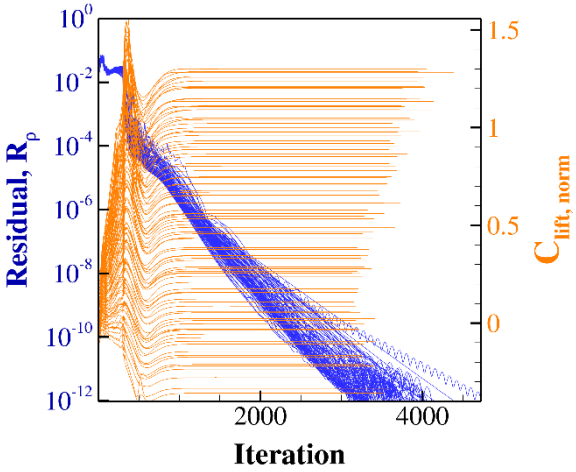

Figure 4: 100 TED-case RANS solutions; AoAs set according to cruise condition for each sample's FL.

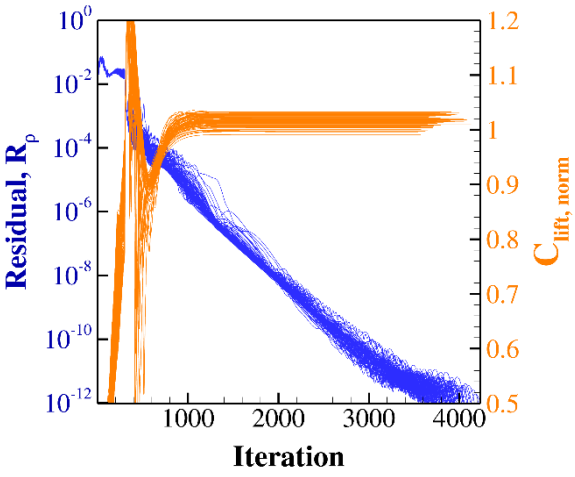

Figure 5: 100 DND-case RANS solutions; AoAs set according to cruise condition for each sample's FL.

5.2. LFD SOLUTIONS

The RANS solutions provided a basis for subsequent computations with LFD. The simulations were run again on a single node each on the DLR CARA Cluster, and took ~2 hours, per ROM, to complete. The solution method used for the LFD solver was

the GMRES [9] method. As a criterion for convergence, a residual reduction of under -9 orders of magnitude was targeted and achieved for all three ROMS. The range of frequencies investigated were from 0 – 40 Hz, which included all viable harmonics to describe an aerodynamic device oscillation such as a simple flap, or in this case a trailing-edge device or a droop-nose device. In simulations themselves, the frequencies were converted to reduced-frequencies, *k* (Eq. 7), which best describe the aerodynamics of the study in question.

The dynamic responses are evaluated as the change of aerodynamic coefficient value with respect to the device deflection angle: $\partial c_l/\partial\delta$, $\partial c_d/\partial\delta$, and $\partial c_m/\partial\delta$ over 200 frequencies from 0 to 40 Hz, for the gust response, trailing-edge and droop-nose device surrogates respectively. The LFD solver itself provides the mentioned aerodynamic coefficient changes as real and imaginary values, which could then be used to calculate the dynamic response magnitude and phase according to Eq. 8 and 9.

As an example, Fig. 6 depicts the frequency response computed by the LFD, portraying the $\partial c_l/\partial\delta$ magnitude and phase changes over the range of frequencies investigated for the TED case. Each curve denotes one snapshot for the ROM, and these LFD solutions formed the database of points for interpolating new values within the surrogate.

$$k = \frac{\omega * l_{ref}}{v_\infty} \tag{7}$$

$$\frac{\partial c_L}{\partial \delta}(\omega) = \sqrt{\left(\frac{\partial \hat{c}_L}{\partial \delta}\right)_{re}^{2} + \left(\frac{\partial \hat{c}_L}{\partial \delta}\right)_{im}^{2}} \tag{8}$$

$$\varphi(\omega) = \tan^{-1}\left(\frac{\left(\frac{\partial \hat{c}_L}{\partial \delta}\right)_{im}}{\left(\frac{\partial \hat{c}_L}{\partial \delta}\right)_{re}}\right) \tag{9}$$

Generally, it is seen that for the trailing-edge flap, the amplitude response drops with increasing frequency. Nevertheless, in the low frequency range below about 5Hz, the amplitude spread depending on the case is quite high providing high expectations on the usability for loads control. The phase response is quite similar for all snapshots.

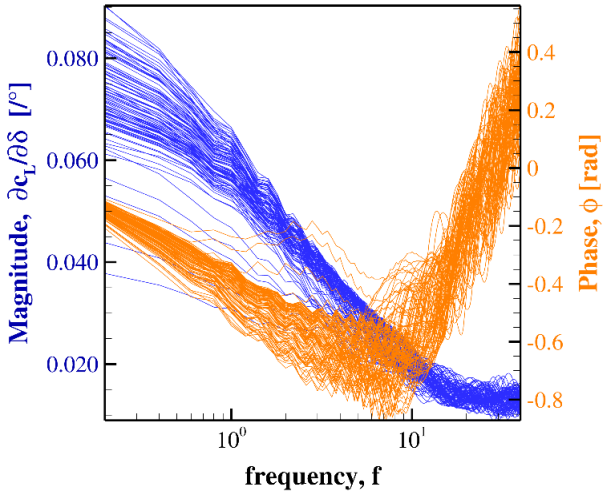

Figure 6: TED case LFD solutions; magnitude and phase for 100 samples over 200 frequencies.

6. SURROGATE QUALITY CHECK: LEAVE-ONE-OUT TEST

To verify the validity of each ROM built upon the snapshots described above, the quality check was conducted via the Leave-One-Out Test. A single sample is removed from the database and the surrogate is required to re-interpolate the missing point. Should the surrogate manage to do so, it would imply two things, namely, that the ROM's capable of reproducing results which reflect the authenticity of high-fidelity simulations, and, that the missing data-point doesn't reduce the ROM's ability to predict correct results. Table 2 summarizes the average relative errors detected by this testing procedure. Despite having a few outliers, the quality of the ROMs is judged as highly adequate for the purpose of this study.

Table 2: Surrogate Quality Check Relative Error [%]

ROM	Average Relative Error [%]	
	Static	Dynamic
Gust	1e-4	2.2e-4
TED	1.12	-1.1e-1
DND	-4.8e-3	-2.7e-1

7. ROM APPLICATION; GUST LOAD ALLEVIATION STUDIES

The prepared ROMs were used for the purpose of dynamic load prediction in line with the requirements of the project. 3 flight cases were investigated (Table 3) and the gust cases were taken from CS-25 §25.341. The angles of attack were established for the transonic cruise condition's target c_l investigated in Section *Simulation: RANS Solutions*. The studies in this section worked not just to investigate the load mitigation capability of the control surfaces in question, but also the predictive

capability of the ROMs themselves. The extremes of the gust-case range outlined in CS-25 §25.341, also forming the extreme edges of the surrogate's parameter space in this work, were therefore used. Should these extreme gust conditions be manageable by the ROMs with reasonable accuracy, the surrogates would be just as reliable for any other value in between.

Table 3: Flight Cases and Gust Conditions for Study

Flight Condition	Ma	FL	AoA	Gust half-wavelength, H	
				10 m	107 m
1	0,83	350	1,193	✓	✓
2	0,85	350	1,052	✓	✓
3	0,83	340	1,185	✓	✓

The following sequence of ROM prognoses were carried out to perform a complete GLA study:

1. The profile's lift coefficient changes due to gust
2. The required TED deflection to counteract the lift increments due to gust
3. The resultant lift variations due to the TED deflection in step .2
4. The resultant lift alleviation
5. The profile's pitching moment changes due to the TED deflection
6. The required DND deflection to counteract the profile's pitching moment increment due to the TED deflection
7. The pitching moment variations due to the DND deflection
8. The resultant profile pitching moment load alleviation
9. The profile's total drag variation due to TED and DND deflections

Each prognosis can be completed by the ROMs in ~1s. Each complete flight case test using the surrogates was completed in ~2-3 minutes. The results of the flight case tests are displayed in Fig. 7-12:

8. DISCUSSION

8.1. Flight Test Cases

The predictions displayed in Fig. 7 - 12 were run according to the flight conditions in Table 3. Each figure displays the sequence listed above in 6 diagrams. The first diagram depicts the incoming gust in terms of the disturbance velocity. The predicted lift change due to the defined vertical gust shape are shown as solid green curves in the time-plot in upper-center of each figure. The highest lift increment in each plot tallies with the gust shape provided.

The required TED deflection profile is predicted by the surrogate in the upper right diagram of each figure. Two cases are investigated: firstly, the theoretical deflection required to fully counteract the gust, and secondly, the deflection profile producible, should the deflection rate and limit be set according to actuator system limitations. A maximum deflection of 15° and 35°/s were set for this purpose. The resultant prognoses by the surrogates in Fig. 7, 8, and 9 for H=10m showed the TED deflections were slightly decelerated along the profiles where the TED deflection rates exceeded the set limit for TED deflection rate. This deceleration however, was not observed in cases for H=107m in Fig. 10, 11, and 12, indicating that the deflection rates for these cases were already within 35°/s. The maximum TED deflection didn't change for any of the cases, since a deflection of 2°-3° were already sufficient to alleviate the lift loads generated by the gust cases studied here. The resultant lift profile following the actions of the TED is displayed as a delta curve in the upper-middle diagram of the figures. For Flight Case 1, 2 and 3 with H=10m, a near 100% lift mitigation capability (>80%) with the TED was possible, while cases for H=107m were able to completely mitigate the lift changes produced by the gust.

A direct consequence of the TED deflection was the airfoil's pitching moment change, shown in the lower-center diagram of each figure as a solid orange curve. The fluctuations seen would influence the aeroelastics of the wing. The required DND deflection for total mitigation of the sectional torsion is predicted in the lower right diagram of each figure as a solid brown curve, while the brown delta curve takes actuator system limitations into account. The total mitigation of the DND considering system limitations is displayed as the orange delta curve in the lower-center diagram for each figure. In this consideration, just around 40% of moment loads could be alleviated at peak gust interaction with the profile for H=10m, while only 20% was manageable for H=107m. Even for gust cases H=10m, the required DND deflection for complete mitigation was already relatively large, ~40°; It is clear then, that for the cases for the larger gust wavelengths (H=107m), implying also a relatively high vertical gust speed, an unrealistically large DND deflection (up to ~70°) would be required to completely mitigate the sectional torque produced by the TED deflection. This directly resulted in a much smaller mitigation capability of the system, when the limitations on the maximum permissible DND deflection are set into the surrogate.

The total drag fluctuations as a result of the two device deflections are shown in the lower-left

diagram in a solid brown curve relative to drag value at cruise displayed as a horizontal dashed brown line. The relative difference between the two are shown as purple lines depicting up to 30% drag fluctuations for gust cases H=10m with respect to the cruise condition, while a relative drag fluctuation up to 70% was observed for gust cases H=107m. For the latter mentioned gust case, the recorded drag variations are large, even with system limitations in place. This should be accounted for when considering overall aerodynamic efficiency and passenger comfort.

8.2. Comparison of Surrogate Predictions vs URANS

The surrogate results for the trailing-edge device reflected the URANS simulations for the same conditions within an accuracy of -2 orders of magnitude (Fig. 13). This showed a rather good predictive capability of the surrogates for such test cases. Since the simulation method of the steady RANS underlying the RANS-LFD procedure is identical to the URANS, differences can be attributed generally to the assumptions made by linearization. Discrepancies at the start and end of the curves are due to the periodicity assumption of the LFD process, which considers a tuned oscillation in the system, as opposed to the URANS simulation, which captures a more realistic scenario of deflection from a stationary position. To minimize this difference, a delay time prior to and post deflection was added into the device deflection profile for surrogate prediction. The difference was thus reduced, but still present and observable to a slight degree. Increasing this pause period further would further reduce this discrepancy.

A larger discrepancy was observed in the case of the droop-nose device, as shown in Fig. 14. It is suspected, that the drooping of the device in the transonic condition caused an increased influence of shocks that weren't captured in the predictions of the surrogate, which is based on an LFD database and thus assumes strict linearity in the flow field for prognosis. Despite this, the differences between the unsteady-RANS results and the surrogate's predictions were still in the range of -2 order of magnitude.

All in all, the predictions produced by the surrogate were satisfactory for the purposes of this study and the extreme gust conditions considered. Such results would still prove useful as first step estimates for further detailed study, i.e, to estimate start values of device deflections in system refinement studies or as system evaluations for flight cases under gust conditions.

The results of the surrogates compared to URANS can also be further improved with a more refined database of higher point density. Time and computational expense should then be considered as a trade-off to result accuracy.

9. CONLUSION

The prepared surrogates proved robust in prognosing load alleviation capabilities of trailing edge and droop-nose devices. The flight case study predictions by the surrogates were comparable with their URANS counterpart and provided valuable information regarding the dynamic behavior of such load control mechanisms, all while saving computational effort and time. A large number of flight conditions can thereby be investigated quickly and efficiently with the prepared ROMs as opposed to studying each flight case separately with standard unsteady CFD techniques. The value of surrogate modelling for aerodynamic research is thus further confirmed by the results and conclusions of this study.

Concerning gust load mitigation with a trailing-edge and a droop-nose device, it can be inferred that complete lift alleviation is possible with the trailing edge device, throughout the range of relevant gust conditions outlined by CS-25 §25.341, namely from H = 10m to 107m. Both extremes of gust wavelengths can be managed by a trailing edge deflection well within the capabilities of an aircraft actuation system. This validates the claim for using a trailing edge device, such as an aileron or flap-tab for the purpose of load alleviation. A lower load mitigation capability, however, is seen by the actuation of the droop-nose-device. Only around 20% to 40% was possible considering the limitations of the actuation system; while complete sectional torque mitigation would require unreasonably large DND deflections. It is therefore a cause for caution when implementing such active gust load alleviation measures, as compensation of these residual sectional moment increments due to TED action would still influence the aerodynamics, aeroelastics, and structure of the wing. A possibility to further alleviate these loads would be to combine TED and DND deflections across the span of the wing, as shown in [10], where further alleviation was possible, though still limited. It is also notable that the results of this study agree with the URANS results of Ullah et.al. [10] for a 3D wing, in terms of device effectiveness in load mitigation. A 3D surrogate modelling study could provide a healthy database of information for the complete gust load mitigation capability of TED and DND deflections for an entire wing. Finally, large changes in drag is a cause for concern in GLA systems, as aerodynamic efficiency and passenger comfort may be compromised.

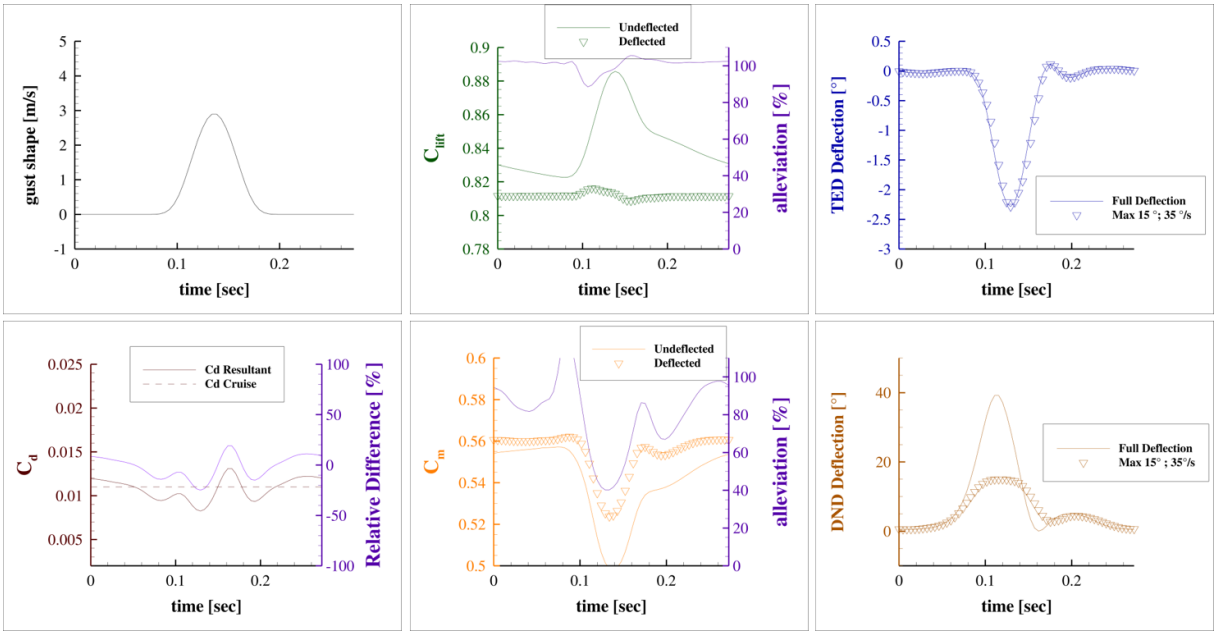

Figure 7: Flight Case 1: Gust-half-wavelength 10m; gust-shape definition (upper-left); lift coefficient prognosis and lift mitigation (upper-center); required TED deflection (upper-right); required DND deflection (lower-right); profile moment due to device deflection and moment load alleviation (lower-center); resultant profile drag due to device deflection and relative drag fluctuation (lower-left).

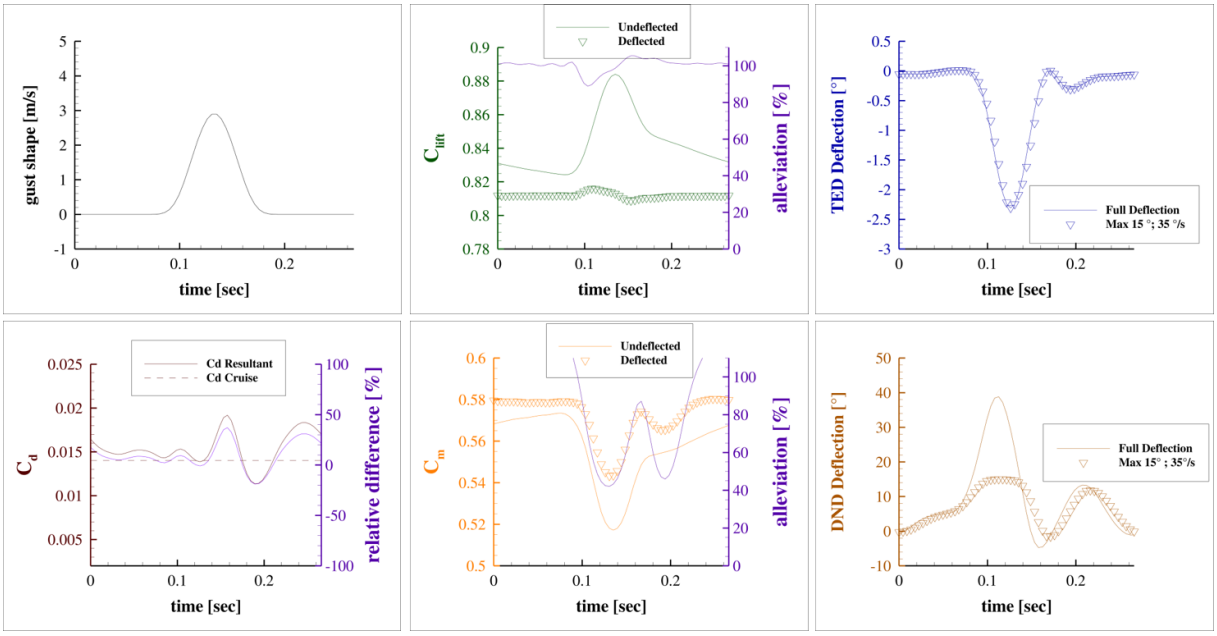

Figure 8: Flight Case 2: Gust-half-wavelength 10m; gust-shape definition (upper-left); lift coefficient prognosis and lift mitigation (upper-center); required TED deflection (upper-right); required DND deflection (lower-right); profile moment due to device deflection and moment load alleviation (lower-center); resultant profile drag due to device deflection and relative drag fluctuation (lower-left).

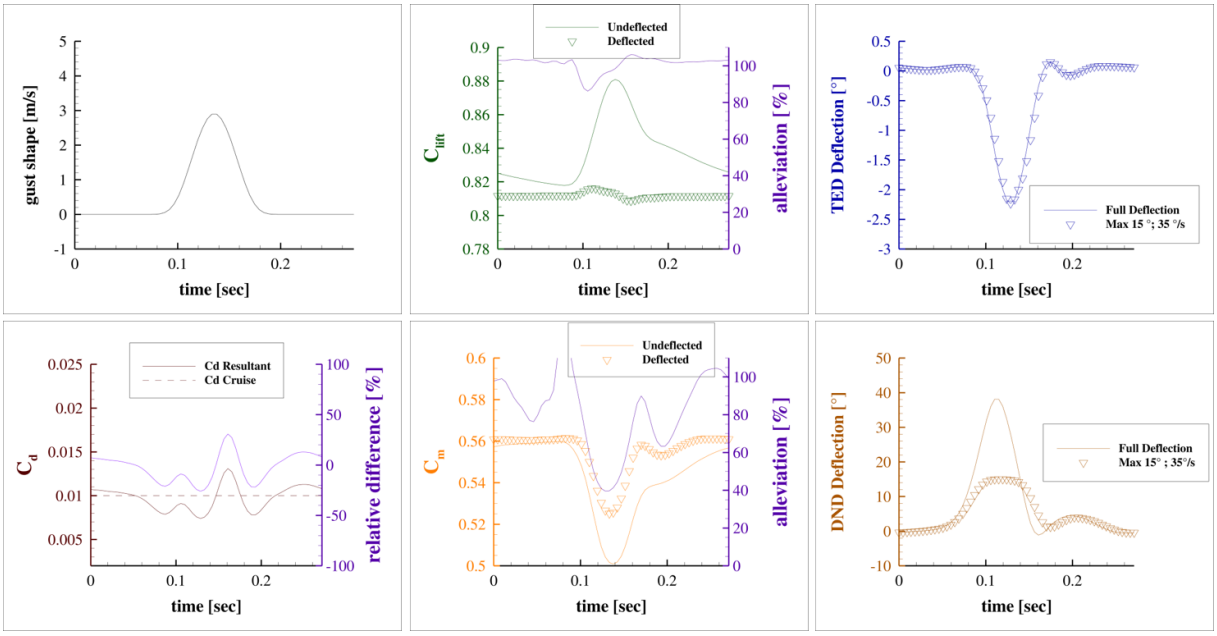

Figure 9: Flight Case 3: Gust-half-wavelength 10m; gust-shape definition (upper-left); lift coefficient prognosis and lift mitigation (upper-center); required TED deflection (upper-right); required DND deflection (lower-right); profile moment due to device deflection and moment load alleviation (lower-center); resultant profile drag due to device deflection and relative drag fluctuation (lower-left).

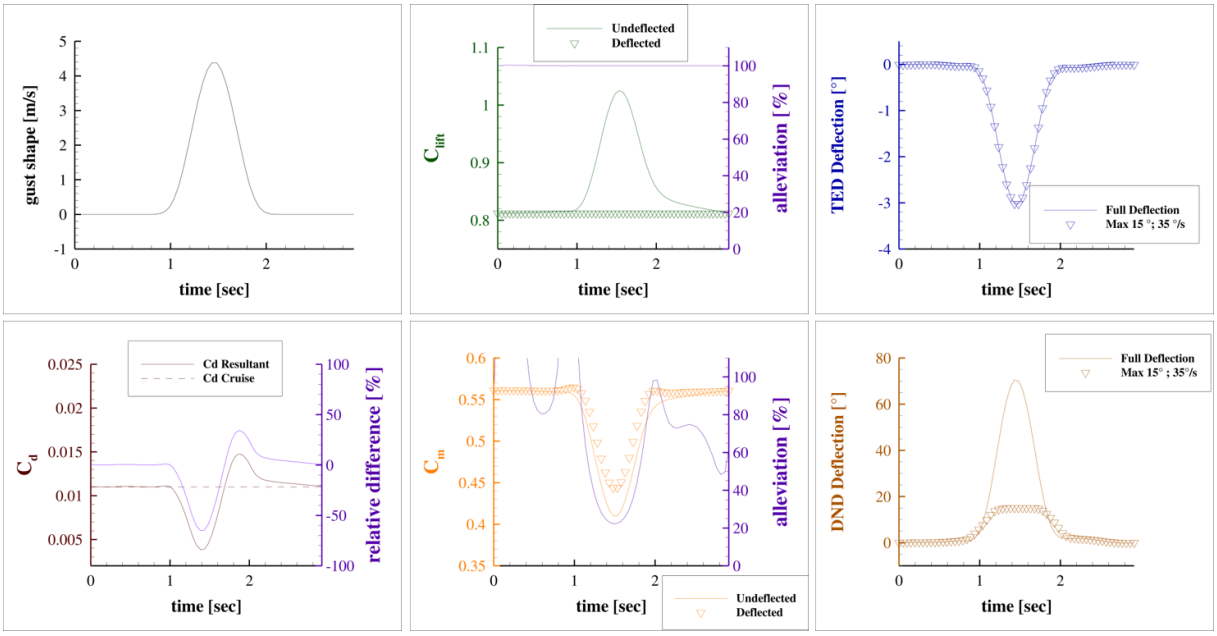

Figure 10: Flight Case 1: Gust-half-wavelength 107m; gust-shape definition (upper-left); lift coefficient prognosis and lift mitigation (upper-center); required TED deflection (upper-right); required DND deflection (lower-right); profile moment due to device deflection and moment load alleviation (lower-center); resultant profile drag due to device deflection and relative drag fluctuation (lower-left).

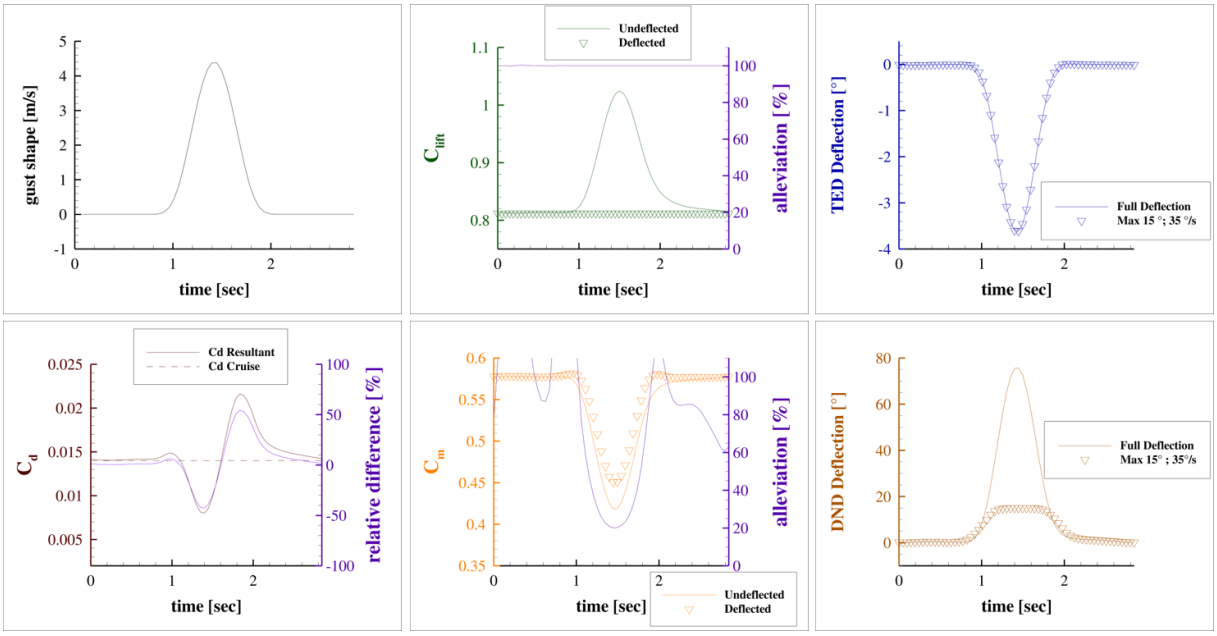

Figure 11: Flight Case 2: Gust-half-wavelength 107m; gust-shape definition (upper-left); lift coefficient prognosis and lift mitigation (upper-center); required TED deflection (upper-right); required DND deflection (lower-right); profile moment due to device deflection and moment load alleviation (lower-center); resultant profile drag due to device deflection and relative drag fluctuation (lower-left).

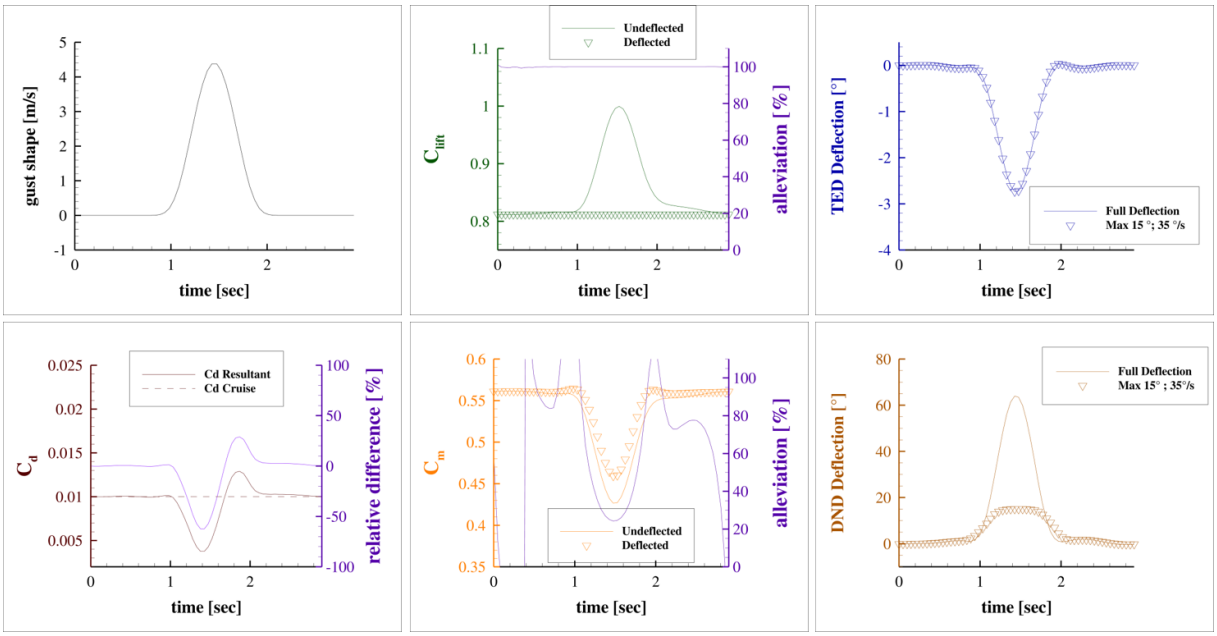

Figure 12: Flight Case 3: Gust-half-wavelength 107m; gust-shape definition (upper-left); lift coefficient prognosis and lift mitigation (upper-center); required TED deflection (upper-right); required DND deflection (lower-right); profile moment due to device deflection and moment load alleviation (lower-center); resultant profile drag due to device deflection and relative drag fluctuation (lower-left).

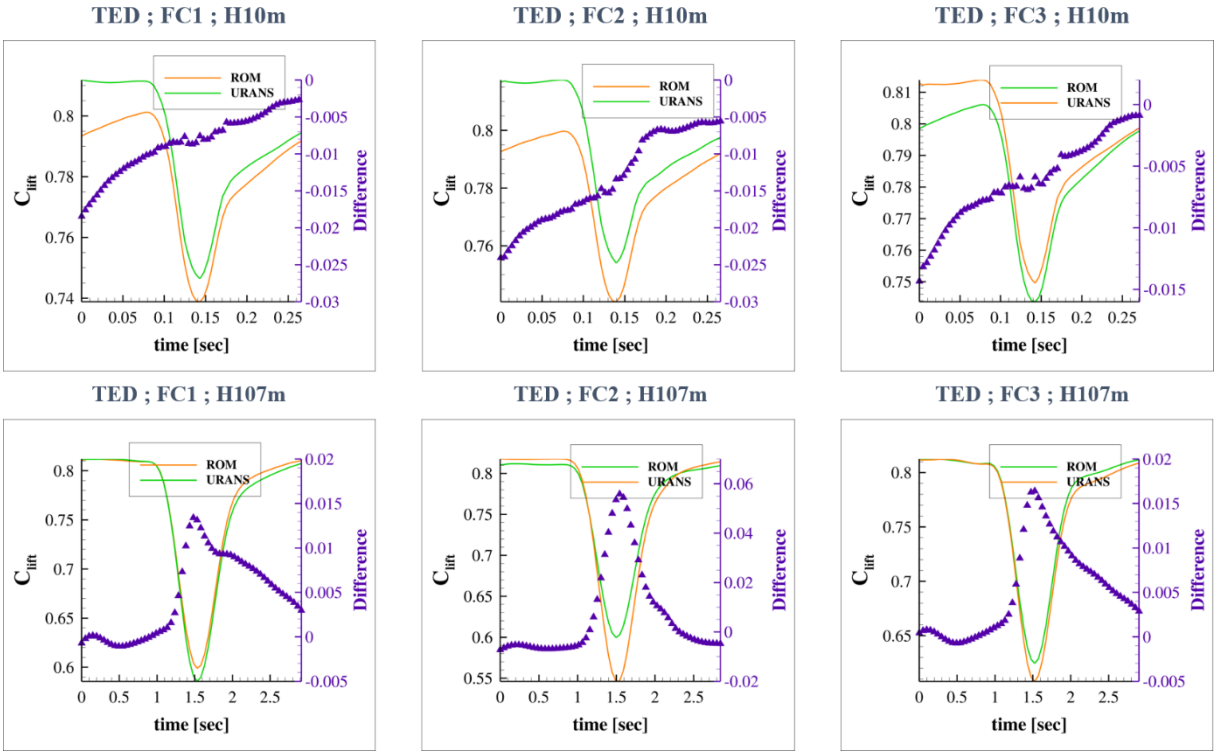

Figure 13: TED ROM predictions vs URANS results for all Flight Cases (FCs)

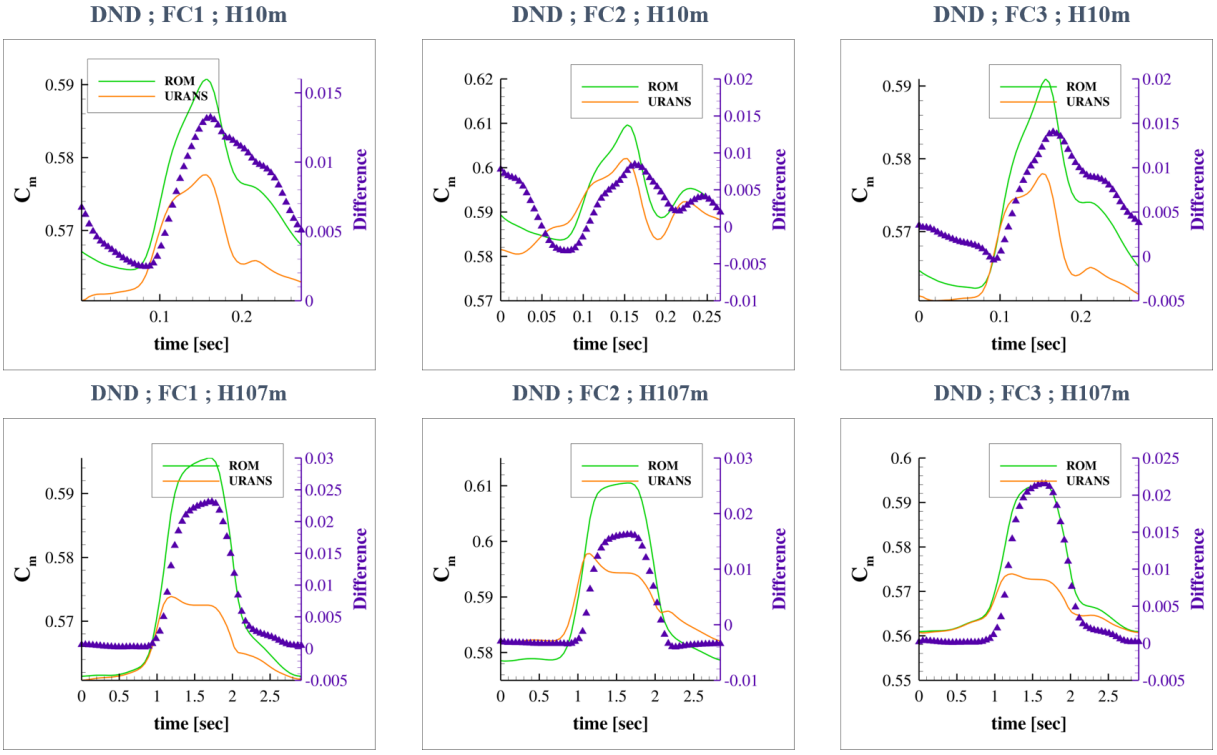

Figure 14: DND ROM predictions vs URANS results for all Flight Cases (FCs)

10. ACKNOWLEDGEMENTS

This work has been funded by the German Ministry of Economic Affairs and Climate Action (BMWK) on decision of the German Parliament in the frame of the INTELWI project (funding reference no. 20A1903L).

11. REFERENCES

1. Bekemeyer, P., et. al. (2022), “Data-driven aerodynamic modeling using the DLR SMARTy Toolbox”, AIAA Aviation 2022 Forum, pp 1-19. doi: 10.2514/6.2022-3899.
2. Berblinger, M., Schlier, C. (1991), “Monte Carlo integration with quasi-random numbers: some experience”, Computer Physics Communications, Vol 66 (2-3), pp.157-166. doi:10.1016/0010-4655(91)90064-R. ISSN 0010-4655.
3. European Union Aviation Safety Agency (2023) Certification Specifications and Acceptable Means of Compliance for Large Aeroplanes, EASA CS-25, Amendment 27.
4. Govindan, K. et.al. (2022), “Modelling aileron and spoiler deflections with the linear frequency domain method (LFD) for subsonic flight conditions”, International Journal of Numerical Method for Heat & Fluid Flow, Vol. ahead-of-print. doi:10.1108/HFF-09-2022-0519
5. Guangqjui, W., et.al. (2015), “Preliminary design of a truss-braced natural-laminar-flow composite wing via aeroelastic tailoring”, ASDJournal, Vol. 3, No. 3, pp. 1-17, doi:10.3293/ASDJ.V313.36.
6. Halton, J.H. (1960), “On the efficiency of certain quasi-random sequences of points in evaluating multi-dimensional integrals” Numerische Mathematik, Vol. 2, pp.84-90.
7. Hübner, A., Reimer, L. (2019), “Gust encounter simulations of a generic transport aircraft and analysis of load alleviation potentials by control surface deflections using a RANS-CFD-based multidisciplinary simulation environment”, AIAA Aviation 2019, doi: 10.2514/6.2019-3198.
8. Kretov, A., Tiniakov, D. (2022), “Evaluation of the mass and aerodynamic efficiency of a high aspect ratio wing for prospective passenger aircraft”, Aerospace 2022, 9, 497, doi:10.3390/aerospace9090497.
9. Saad, Y., Schultz, M., (1986), “GMRES: A generalized minimal residual algorithm for solving nonsymmetric linear systems”, SIAM Journal on Scientific and Statistical Computing, Vol. 7, No.3, doi:10.1137/0907058.
10. Ullah, J., Lutz, T. (2022), “Active gust load alleviation by means of steady and dynamic trailing and leading-edge flap deflections at transonic speeds”, AIAA SciTech Forum, doi:10.2514/6.2022-1334.
11. Widhalm, M., Thormann, R. (2017), “Efficient evaluation of dynamic response data with a linearized frequency domain solver at transonic separated flow conditions”, AIAA Aviation and Aeronautics Forum and Exposition, doi:10.2514/6.2017-3905.
12. Wu, Z., Cao, Y., Ismail M. (2019), “Gust loads on aircraft”, *The Aeronautical Journal*, Vol. 123 No. 1266, pp. 1216-1274, doi:10.1017/aer.2019.48.
13. Xu, J. (2012), “Aircraft design with active load alleviation and natural laminar flow”, Ph.D dissertation, *Stanford University, California*, http://purl.stanford.edu/hz528zb1688.